MICROBIOLOGY

Creation of a macrolide antibiotic against non-tuberculous *Mycobacterium* using late-stage boron-mediated aglycon delivery

Yuka Isozaki[1], Takumi Makikawa[1], Kosuke Kimura[1], Daiki Nishihara[2], Maho Fujino[2], Yoshikazu Tanaka[2,3], Chigusa Hayashi[4], Yoshimasa Ishizaki[4], Masayuki Igarashi[4]*, Takeshi Yokoyama[2,3]*, Kazunobu Toshima[1]*, Daisuke Takahashi[1]*

Non-tuberculous mycobacteria (NTM) is gaining clinical recognition as a recently emerging pulmonary pathogen. *Mycobacterium avium* complex (MAC), the most common NTM, is the cause of pulmonary MAC disease. Currently, the macrolide azithromycin (AZM) is the standard first-line antibiotic for treatment of the disease. However, the rise of drug-resistant MAC necessitates the development of alternative therapeutics. Here, we present a late-stage boron-mediated aglycon delivery strategy for selective modification of AZM, generating a library of potential anti-MAC drugs designated KU01 to KU13. Screening of KU01 to KU13 revealed that KU13 exhibited enhanced antimicrobial activity against wild-type and macrolide-resistant MAC compared to AZM. Cryo–electron microscopy analysis indicated that the inserted tercyclic moiety of KU13 formed a robust anchor on the bacterial ribosome, creating a binding pocket with base flipping of U2847, potentially bypassing the standard mechanism of macrolide resistance. These results position KU13 as a promising lead for therapeutics against macrolide-resistant MAC.

INTRODUCTION

Non-tuberculous mycobacteria (NTM), a group of mycobacterial species other than *Mycobacterium tuberculosis* and *M. leprae*, are known as opportunistic pathogens that most frequently invade the lungs, skin, soft tissues, and lymph nodes. In particular, the lungs are the most-commonly affected organ, and the disease is known to occur in people with anatomical or structural abnormalities of the airways/lungs, such as bronchiectasis, chronic obstructive pulmonary disease, and cystic fibrosis. NTM encompasses more than 190 species that are found worldwide; mycobacteria of this class are ubiquitously present in water, soil, livestock, wildlife, and food. NTM diseases require a long treatment period, have a high relapse rate, and have been increasing in incidence in recent years, making such conditions a major global issue (*1*). In addition, the incidence of NTM disease in immunocompetent individuals without lung disease has increased considerably over time (*1*, *2*). In Japan, the incidence of NTM infection increased from 5.7 to 14.7 per 100,000 person-years between 2007 and 2014 (*3*). Similar data have been reported in several studies conducted in Europe, the United States, and Asia.

One of the important shared findings from these epidemiological studies is that the primary pathogens in Japanese patients typically are members of the *Mycobacterium avium* complex (MAC), a group of two mycobacterial species, *M. avium* and *M. intracellulare* (*4*). Similar observations have been reported in other countries and regions, including Korea, Canada, Australia, and the Pacific coastal region of China. In Japan, MAC accounts for approximately 90% of NTM-related disease cases; approximately 90% of these cases are pulmonary MAC disease. Recent studies in Japan and the United States have shown a notable increase in the incidence of NTM-related diseases in middle-aged and older women lacking any previous underlying diseases.

Treatment of pulmonary MAC is based on combination chemotherapy, and treatment is required for at least 12 months after culture negativity. Guidelines of the American Thoracic Society (ATS), the European Respiratory Society (ERS), the European Society for Clinical Microbiology and Infectious Diseases (ESCMID), and the Infectious Diseases Society of America (IDSA) strongly recommend a three-drug regimen including a macrolide for patients with macrolide-susceptible MAC pulmonary disease (*5*). Combination therapy with three oral antibiotics, azithromycin (AZM), rifampicin, and ethambutol, is currently considered the standard of care (*6*, *7*). The only key drug for the treatment of MAC pulmonary disease is a macrolide, typically consisting of AZM or clarithromycin (CAM) (Fig. 1). The other two antibiotics, rifampicin and ethambutol, have low bactericidal effects when used as monotherapies, but are thought to help prevent the acquisition of macrolide resistance when administered in combination with a macrolide (compared to the case when macrolides are used alone) (*6*).

Currently, the ATS/ERS/ESCMID/IDSA guidelines recommend drugs for MAC treatment regimens only based on the indications of existing antituberculous and other antimicrobial drugs (*5*, *8*). As a result, there are limited options for the treatment of macrolide-resistant MAC, with possible regimens consisting of amikacin liposomal inhalation suspension and streptomycin injection (*2*). Moreover, the emergence of drug-resistant bacteria remains a major clinical challenge (*7*). Treatment outcomes for macrolide-resistant MAC lung disease are poor despite combination therapy with multiple antibiotics and surgical resection, resulting in an overall 1-year mortality rate of 10% (*9*). Thus, development of alternative therapeutic agents that are effective against macrolide-resistant strains is urgently required.

[1]Department of Applied Chemistry, Faculty of Science and Technology, Keio University, 3-14-1 Hiyoshi, Kohoku-ku, Yokohama 223-8522, Japan. [2]Graduate School of Life Sciences, Tohoku University, 2-1-1 Katahira, Aoba-ku, Sendai, Miyagi 980-8577, Japan. [3]The Advanced Center for Innovations in Next-Generation Medicine (INGEM), Tohoku University, 2-1 Seiryo-machi, Aoba-ku, Sendai, Miyagi 980-8573, Japan. [4]Institute of Microbial Chemistry (BIKAKEN), 3-14-23 Kamiosaki, Shinagawa-ku, Tokyo 141-0021, Japan.
*Corresponding author. Email: igarashim@bikaken.or.jp (M.I.); takeshi.yokoyama.d1@tohoku.ac.jp (T.Y.); toshima@applc.keio.ac.jp (K.T.); dtak@applc.keio.ac.jp (D.T.)

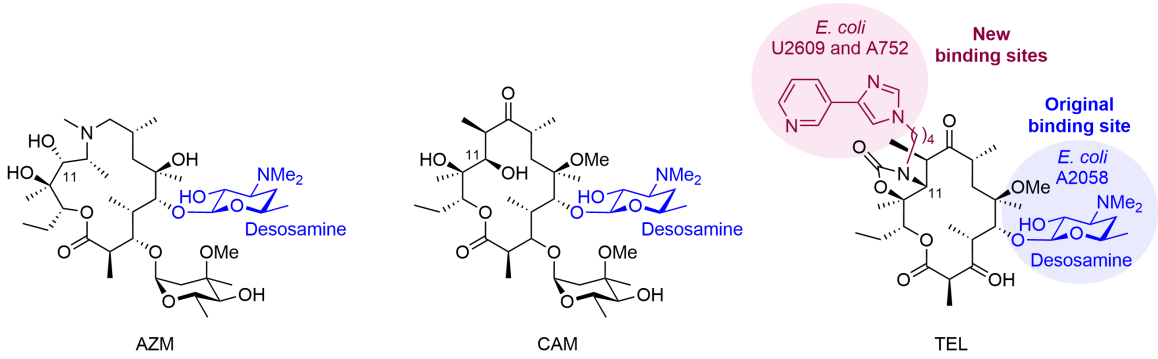

Fig. 1. Chemical structures of macrolide antibiotics. Structures of azithromycin (AZM), clarithromycin (CAM), and telithromycin (TEL). The C-11 sidechain of TEL (brown) interacts with residues U2609 and A752 of the *E. coli* 23*S* rRNA (*12*), representing a new ribosome binding compared to the A2058 residue of the *E. coli* 23*S* rRNA that is targeted by the desosamine moiety (blue) shared among the macrolides.

Bacteria synthesize proteins using ribosomes and export the resulting proteins through the nascent peptide exit tunnel (NPET) in the ribosome. In contrast, macrolide antibiotics express their antibacterial activity by binding to peptide tunnels neighboring the peptidyl transferase center (PTC) in the bacterial 23*S* rRNA, causing translation arrest in the presence of nascent peptide chains with specific amino acid sequences (*10*, *11*). The 23*S* rRNA consists of approximately 3000 nucleotides, and most macrolide antibiotics are known to bind to adenine at positions 2058 and 2059 (*Escherichia coli* numbering) via the antibiotics' desosamine moiety (*12*). NTM develops macrolide resistance primarily through the efflux of macrolide antibiotics by efflux proteins (*13*–*15*), ribosomal methylation by the product of the *erm* gene (*16*, *17*) and nucleotide mutations within the 23*S* rRNA (*18*). Currently reported rRNA mutations include mutation of A2058 and A2059 to guanine (i.e., A2058G and A2059G; *E. coli* numbering); such changes are selected by exposure to either AZM or CAM (*19*). Either of these individual mutations disrupts the crucial interaction of the 23*S* rRNA with the desosamine moiety of these macrolide antibiotics.

Other work has shown that telithromycin (TEL), a third-generation macrolide antibiotic approved in 2004, exhibits distinctive sites of binding to the *E. coli* 23*S* rRNA, though not to the 23*S* rRNA from NTM (*20*). X-ray crystallography of TEL complexed with the *E. coli* ribosome demonstrates bindings at U2609 and A752 via the C-11 substituent of TEL, while maintaining the hydrogen bond between TEL's desosamine moiety and A2058 (*12*). In addition to TEL, a class of fully synthetic ketolides and azalides incorporating triazole side chains has exhibited remarkable antimicrobial efficacy against specific macrolide-resistant bacterial strains (*21*, *22*). On the basis of this observation, we hypothesized that the introduction of a side chain at C-11 of AZM would result in the formation of an additional interaction with the ribosome, thereby enhancing the binding affinity of AZM against ribosomes from macrolide-resistant NTM.

In other work, regio- and stereoselective glycosylation reactions using organoboron compounds and other reagents have been developed (*23*, *24*). However, we have recently reported the modification of glycosides via a regio- and 1,2-*cis*-stereoselective glycosylation reaction catalyzed solely by boronic acids under mild conditions, a process that we have designated boron-mediated aglycon delivery (BMAD) (*25*–*36*) (Fig. 2A). In this reaction, boronic ester prepared from diol acceptor **2** and boronic acid **3** activates the 1,2-anhydro donor **1** under mild reaction conditions. The boron-bound oxygen atom in the resulting tetracoordinate boronate ester exhibits increased nucleophilicity. Subsequent intramolecular glycosylation from the oxygen atom closer to the anomeric center in the favored transition state provides the 1,2-*cis* glycoside **4** with high regio- and 1,2-*cis*-stereoselectivities, in an S_Ni manner. In addition, we demonstrated that the BMAD method can be applied to the site-selective and late-stage glycosylation of nonprotected natural glycosides such as lanatoside C (LanC), a molecule that bears eight free hydroxy groups (Fig. 2B) (*36*). In our previous study, we reported an efficient strategy for the preparation of chemical probes of LanC by a reaction sequence consisting of (i) a BMAD reaction with a N_3-functionalized donor (compound **5**), (ii) deprotection of triisopropyl silane (TIPS) groups, and (iii) a Huisgen cycloaddition reaction. In light of our previous findings, we focused on the 1,2-diol structure, this time within a macrolide ring instead of a glycoside, i.e., at C-11 and 12 of AZM. Specifically, we anticipated that late-stage BMAD would target the C-11,12-diol and the glycosylation would proceed exclusively at the C-11 hydroxy group to provide an α(1‴, 11) glycoside, thereby providing the desired C-11–modified AZM derivatives (Fig. 2C). It should be noted that previous work has demonstrated site-selective glycosylations of 14-membered macrolides at the C-11 mono-ol position (*37*), though none of its application to the C-11,12 diol position in macrolides has been reported. The sequence of BMAD, deprotection, and Huisgen cycloaddition with a range of alkynes was expected to result in the production of a library of AZM derivatives (Fig. 2D). In the present study, chemical modification of AZM was performed to develop AZM derivatives as potential lead compounds for macrolide-resistant anti-MAC drugs.

RESULTS

Synthesis of AZM derivatives KU01 to KU13

Our initial step was to develop the late-stage BMAD strategy for the chemical modification of AZM. This process involved a reaction between AZM and sugar donors in the presence of a boronic acid catalyst (compound **3**). First, we used ^{1}H–nuclear magnetic resonance (NMR) to investigate the formation of the boronic ester of AZM when exposed to **3** (fig. S1). NMR spectral analysis of a solution of AZM and **3** indicated a downfield chemical shift of AZM H-11 from 3.69 to 4.40 parts per million (ppm), C-11 from 73.4 to 87.2 ppm, and C-12 from 74.1 to 85.7 ppm, which implied the coordination of **3** to the C-11,12-diol. As we expected from this result, when glucose donor **1** was used in the BMAD reaction

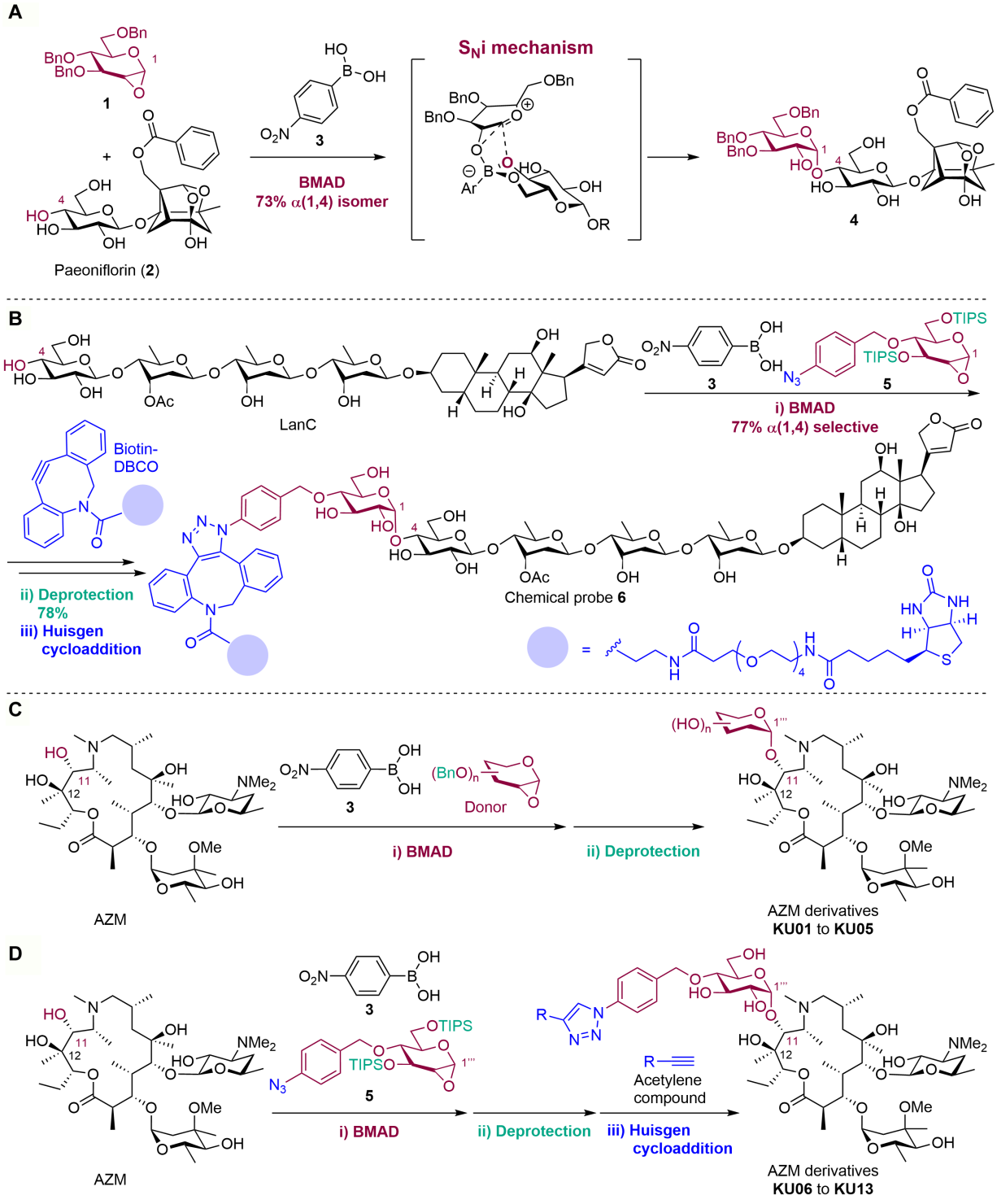

Fig. 2. Application of BMAD method to the synthesis of AZM analogs. (**A**) Highly stereo- and regioselective glycosylation of a nonprotected glycoside using boronic acid catalyst **3** (*29*). (**B**) A chemical probe of lanatoside C (LanC) was synthesized using the late-stage BMAD method (*36*). (**C**) Development of a late-stage BMAD method to selectively introduce sugar moieties at C-11 of AZM, permitting synthesis of AZM derivatives designated **KU01** to **KU05**. (**D**) Efficient three-step reaction sequence of (i) late-stage BMAD reaction, (ii) deprotection reaction, and (iii) Huisgen cycloaddition, permitting synthesis of AZM derivatives **KU06** to **KU13** using azido or triazole substituents. Bn, benzyl; TIPS, triisopropylsilyl; DBCO, dibenzylcyclooctyne; Ac, acetyl.

with AZM, using 0.2 equivalents of **3** in a mixed solvent of acetonitrile (MeCN) and dimethyl sulfoxide (DMSO) at room temperature, the glycosylation reaction proceeded with a high yield of 86% and excellent C-11 selectivity and 1,2-*cis*-stereoselectivity (Fig. 3A). Here, the C-11 selectivity was confirmed by the heteronuclear multiple bond correlation between the C-11 of AZM and the anomeric hydrogen atom (H-1‴) of the glucosyl moiety, while the 1,2-*cis*-α-glycosidic bond was identified by the coupling constant $J_{1''',2'''}$, which was calculated to be 2.5 Hz on the ^{1}H-NMR spectrum (fig. S2). Subsequent deprotection of the benzyl group catalyzed by $Pd(OH)_2/C$ in a H_2 atmosphere afforded **KU01**, in which glucose was introduced at C-11 of AZM. Incorporation of various sugar moieties was achieved under a similar sequence providing complete regio- and 1,2-*cis*-stereoselectivity. The presence of 1,2-*cis*-β-glycosidic linkages was confirmed by analyzing the J_{CH} coupling constant between the anomeric carbon and hydrogen atoms. Reported J_{CH} values typically reach approximately 170 Hz for α-anomers and 160 Hz for β-anomers (*38*). Consistent with these expectations, hetereonuclear single quantum coherence spectral analysis of the synthesized derivatives revealed J_{CH} values of 158.5 Hz for the mannoside unit and 161.5 Hz for the rhamnoside unit, confirming the 1,2-*cis*-β-selectivity of the glycosidic linkages (fig. S3). This process provided AZM derivatives **KU02** to **KU05**, thereby establishing an efficient late-stage BMAD strategy for the chemical modification of AZM.

Having successfully established the late-stage BMAD method for AZM, our next step was to synthesize a library of AZM derivatives in which glucose moieties with various functional groups were introduced at the C-11 of AZM. The molecular design incorporated terminal aromatic rings and alkyl amines, to foster π-π stacking and hydrogen bonding with nucleosides within the macrolide's ribosome binding site, which was expected to potentiate the molecule's antibacterial efficacy. The BMAD reaction between AZM and an azidobenzylated glucose donor **5** was investigated using the established conditions (Fig. 3B). The reaction proceeded smoothly to afford **KU06** at a high yield of 89% and with complete C-11 selectivity and 1,2-*cis*-stereoselectivity. **KU06** then was desilylated using tetra-*n*-butylammonium fluoride (TBAF) in tetrahydrofuran (THF) solvent to provide **KU07**. Successive Huisgen cycloaddition with various acetylene compounds furnished glucose-AZM derivatives **KU08** to **KU13** at good yields (Fig. 3C).

MIC assay of AZM derivatives KU01 to KU13

To evaluate the potency of our newly synthesized AZM derivatives **KU01** to **KU13**, minimum inhibitory concentration (MIC) assays were performed against *M. avium* and *M. intracellulare* strains, as well as against respective macrolide-resistant strains (Table 1). AZM and TEL were used as controls. AZM exhibited antimicrobial activity with MIC ≤1 μg ml^{-1} against wild-type MAC but not against macrolide-resistant MAC strains (*M. avium*. subsp. *avium* B-1657 and *M. intracellulare* B-1639) with MIC >32 μg ml^{-1}. In contrast, TEL did not demonstrate antimicrobial activity against macrolide-resistant *M. intracellulare* with MIC of 32 μg ml^{-1} but did exhibit antimicrobial activity against both wild-type MAC (MIC ≤1 μg ml^{-1}) and macrolide-resistant *M. avium* (MIC of 2 μg ml^{-1}). Among the AZM derivatives **KU01** to **KU05**, which are modified with various sugars, and **KU06** and **KU07**, which are modified with azidobenzylated glucose, none were active against macrolide-resistant *M. intracellulare*, expressing MIC ≥32 μg ml^{-1}. In contrast, **KU07** was found to exhibit lower MIC values compared to AZM, not only against wild-type *M. avium* and *M. intracellulare* (MIC values of 0.5 and 0.125 μg ml^{-1}, respectively, for **KU07** compared to MIC values of 1 and 0.25 μg ml^{-1}, respectively, for AZM) but also against macrolide-resistant *M. avium* (MIC of 16 μg ml^{-1} for **KU07** compared to MIC of >32 μg ml^{-1} for AZM), validating the strategy of incorporating azido substituents at the C-11 of AZM. Furthermore, the results obtained with AZM derivatives **KU08** to **KU13** showed that **KU11** and **KU13**, both harboring a pyridine substituent, displayed similar MIC values to TEL, and lower MIC values than AZM against wild-type MAC, with MIC values for **KU11** being 0.5 and **KU13** being 0.25 μg ml^{-1} against *M. avium*, and MIC values for both **KU11** and **KU13** being 0.125 μg ml^{-1} against *M. intracellulare*. In terms of macrolide-resistant strains, the results demonstrated that **KU13** exhibited MIC values that were superior to that of TEL by twofold against macrolide-resistant *M. avium* (MIC of 1 μg ml^{-1}), and by fourfold against macrolide-resistant *M. intracellulare* (MIC of 8 μg ml^{-1}). These findings indicated that, compared to AZM, **KU13** exhibits superior antimicrobial activity against both wild-type and macrolide-resistant MAC. To elucidate the effect of the terminal *para*-pyridine moiety on **KU13**, **KU14** with a simple benzene ring instead of the pyridine ring was synthesized and evaluated for antibacterial activity against *Mycobacterium* species (see table S1). Here, **KU14** expressed similar MIC values to TEL against macrolide-resistant *M. Intracellulare* (MIC of 32 μg ml^{-1}), highlighting the importance of the *para*-pyridine moiety on activity of **KU13** against macrolide-resistant *M. Intracellulare*.

Subsequently, MIC assays were conducted against a strain of *M. tuberculosis* var. Bacille Calmette-Guérin (BCG), a live vaccine strain for tuberculosis that has recently been reclassified as *M. tuberculosis* (*39*). Both AZM and TEL displayed antimicrobial activity with MIC values of 2 and 0.125 μg ml^{-1}, respectively, against *M. tuberculosis*. Derivatives **KU01** to **KU05**, some of which (**KU02**, **KU04**, and **KU05**) bear specific sugar moieties, demonstrated lower MIC values (1, 0.0312, and 1 μg ml^{-1} respectively) compared to AZM. However, **KU08** to **KU13** exhibited even lower MIC values (≤0.5 μg ml^{-1}), indicating that the introduction of a triazole component provides superior activity. Furthermore, **KU13** demonstrated lower MIC (0.0312 μg ml^{-1}) than did TEL (0.125 μg ml^{-1}), emphasizing **KU13**'s activity against the *Mycobacterium* species.

To investigate potential pathogen selectivity, MIC assays also were performed against multiple strains of *E. coli*. While AZM and TEL displayed potent antibacterial activity against *E. coli* displaying MIC values ≤1 μg ml^{-1}, **KU01** to **KU13** exhibited higher MIC values of ≥1 μg ml^{-1} (compared to AZM and TEL) against *E. coli*. MIC assays were further conducted against a panel of other gram-positive and gram-negative bacteria, in which **KU01** to **KU13** mostly displayed higher MIC values compared to AZM and TEL (see table S2). This finding revealed **KU13** to be selectively effective against *Mycobacterium* species.

Translation inhibition assay using an in vitro reconstituted cell free system

The enhancement of antibiotic activity through semisynthetic approaches has led to remarkable advances in antibacterial efficacy (*40*–*42*). The development of the third generation of macrolides, the ketolides, with the insertion of bulky chemical modifications, has increased the efficacy of macrolides compared to the parent compounds (*10*). These extended motifs successfully form additional

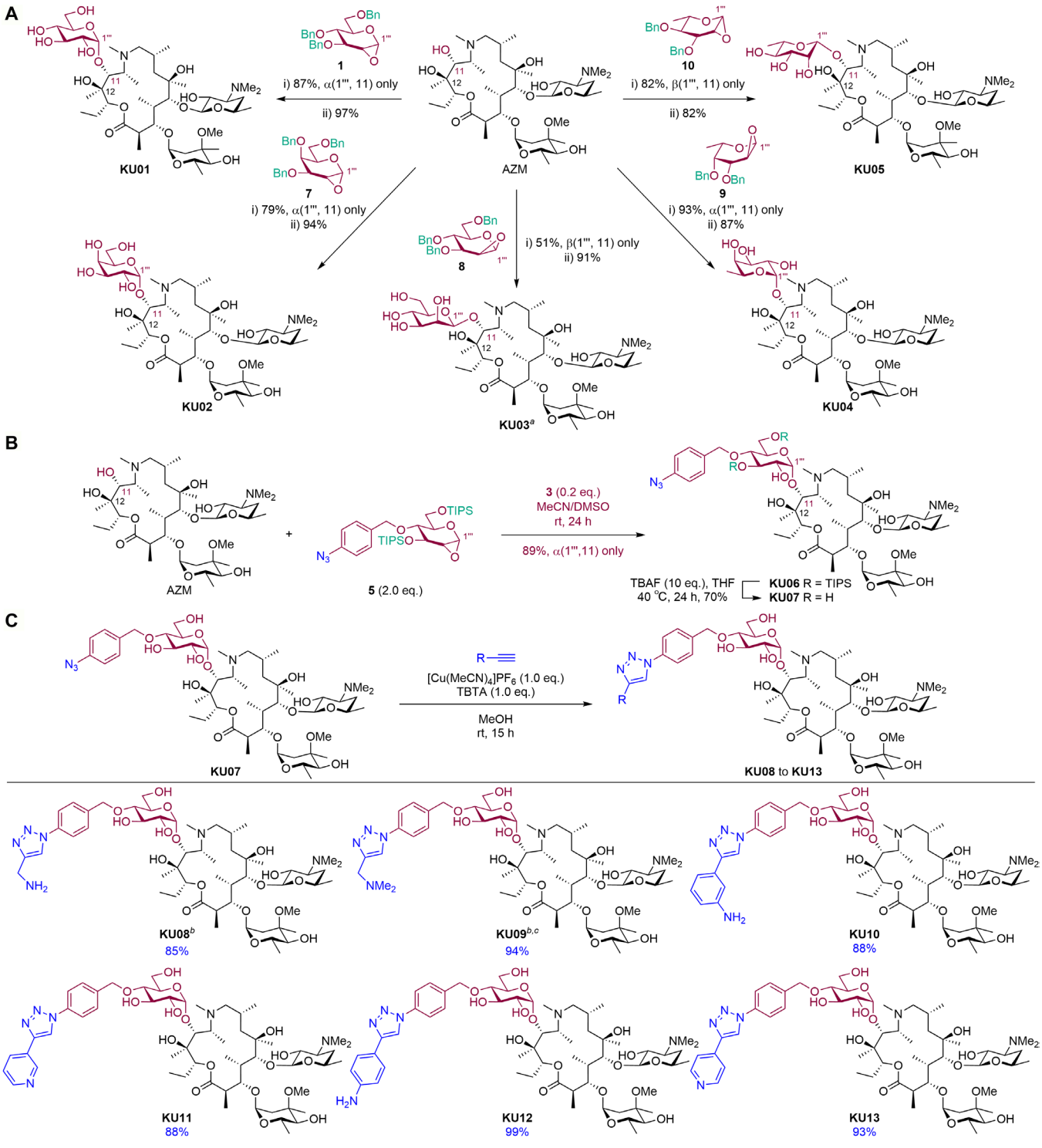

Fig. 3. Synthesis of AZM derivatives KU01 to KU13 using the late-stage BMAD method. (**A**) Various sugar moieties were introduced at C-11 of AZM to provide **KU01** to **KU05**. (i) Donor (2.0 eq.), boronic acid (compound **3**) (0.2 eq.), MeCN/DMSO, room temperature (rt), 24 hours; (ii) H_2 (7 atm), $Pd(OH)_2/C$ [200 weight % (wt %)], EtOAc/MeOH, HCOOH (2 wt %), 4 hours. [a]Donor (3.0 eq.) was used. (**B**) BMAD reaction of AZM and **5**, followed by desilylation to afford **KU07**. (**C**) Huisgen cycloaddition reaction to provide **KU08** to **KU13**. [b]Reaction conditions of $CuSO_4.5H_2O$ (4.0 eq.), Na-ascorbate (1.0 eq.), THF/H_2O, rt, 18 hours was used. [c]$CuSO_4.5H_2O$ (2.0 eq.) were used. MeCN, acetonitrile; DMSO, dimethyl sulfoxide; TBAF, tetra-*n*-butylammonium fluoride; THF, tetrahydrofuran; TBTA, tris[(1-benzyl-1*H*-1,2,3-triazol-4-yl)methyl]amine; MeOH, methanol; EtOAc, ethyl acetate.

interactions with ribosomes (*43*). To investigate the effect of the glucose-tercyclic insertion on translation inhibition by AZM derivatives, we measured green fluorescent protein (GFP) production in a reconstituted cell-free translation system (the PURE system) in the presence of different concentrations of macrolides (Fig. 4) (*44*). Translation inhibition due to the addition of **KU13** was compared with the effect of AZM. Although macrolides selectively inhibit translation in specific amino acid sequence contexts rather than bulk protein synthesis, known as "plug-in-the-bottle" model, for simplicity, we compared global translation inhibition by **KU13** to that by AZM (*11*, *45*). As the concentration of AZM in the PURE system increased, the accumulation of GFP was attenuated due to global translation inhibition (Fig. 4A). Translation inhibition was first observed at 12.5 nM AZM, and this effect increased as the concentration of AZM was further increased, until translation was completely abolished at a concentration of 400 nM AZM (Fig. 4A). A stronger effect was seen with **KU13** (Fig. 4B). As for AZM, the translation inhibition was first observed at 12.5 nM **KU13**; however,

Table 1. MIC assay of AZM derivatives to against MAC, *M. tuberculosis*, and *E. coli*. KU01 KU13 Minimum inhibitory concentration (MIC) assays were performed with *M. avium* and *M. intracellulare* strains, as well as against their corresponding macrolide-resistant strains; with *M. tuberculosis*; and with multiple strains of *E. coli*. The resulting MIC values are expressed in units of μg ml^{-1}.

		MIC (μg ml^{-1})								
Test strains	**23*S* rRNA (*E. coli* numbering)**	**AZM**	**TEL**	**KU01**	**KU02**	**KU03**	**KU04**	**KU05**	**KU06**	**KU07**
M. avium subsp. *avium* ATCC 25291	Wild type	1	1	4	4	4	1	4	>32	0.5
M. avium subsp. *avium* B-1657	A2059C	>32	2	>32	>32	>32	8	>32	32	16
M. intracellulare JCM6384	Wild type	0.25	0.125	1	2	0.5	0.25	2	16	0.125
M. intracellulare B-1639	A2058C	>32	32	>32	>32	>32	>32	>32	32	32
M. tuberculosis var. BCG Tokyo 172–2	Wild type	2	0.125	2	1	8	0.0312	1	>32	1
E. coli CAG 12184	Wild type	0.5	1	32	32	32	4	8	>64	2
E. coli BEM11	Wild type	0.5	1	16	16	16	2	4	>64	2
E. coli BE1121	Wild type	0.5	0.5	16	16	16	1	4	>64	1
E. coli BE1186	Wild type	0.5	1	16	16	16	2	4	>64	1
Test strains	**23*S* rRNA (*E. coli* numbering)**	**AZM**	**TEL**	**KU08**	**KU09**	**KU10**	**KU11**	**KU12**	**KU13**	
M. avium subsp. *avium* ATCC 25291	Wild type	1	1	2	1	0.5	0.5	1	0.25	
M. avium subsp. *avium* B-1657	A2059C	>32	2	1	2	4	0.5	8	1	
M. intracellulare JCM6384	Wild type	0.25	0.125	0.25	0.25	0.5	0.125	0.25	0.125	
M. intracellulare B-1639	A2058C	>32	32	32	>32	32	32	32	8	
M. tuberculosis var. BCG Tokyo 172–2	Wild type	2	0.125	0.125	0.25	0.25	0.125	0.5	0.0312	
E. coli CAG 12184	Wild type	0.5	1	4	4	4	2	4	2	
E. coli BEM11	Wild type	0.5	1	2	4	2	2	2	2	
E. coli BE1121	Wild type	0.5	0.5	2	2	2	1	2	2	
E. coli BE1186	Wild type	0.5	1	4	4	2	2	2	2	

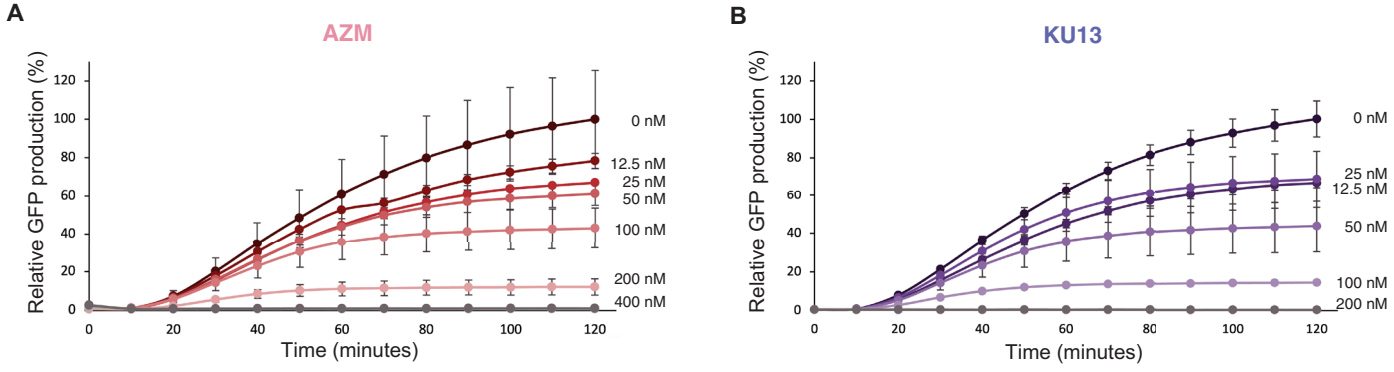

Fig. 4. Translation inhibition assay using in vitro reconstituted cell-free translation system. Green fluorescent protein (GFP) accumulation in the in vitro reconstituted cell-free translation system was monitored in the presence of AZM (**A**) (red) and **KU13** (**B**) (blue). GFP levels in the presence of the various indicated concentrations of AZM and **KU13** were monitored over 120 min. In vitro translation inhibition assays were performed in triplicate, and the averaged values were plotted with their SD.

attenuation was stronger than that observed with AZM (Fig. 4B). Last, at a concentration of 200 nM **KU13**, translation was completely abolished (Fig. 4B). Therefore, our in vitro translation inhibition experiment showed that semisynthetic modification of AZM to generate **KU13** potentiates translation inhibition.

Single-particle cryo-EM reveals KU13 binding at the NPET with associated structural rearrangements of the ribosome

To obtain structural insights into how the chemical modifications incorporated into **KU13** provide higher translation inhibition, the **KU13**-bound *M. tuberculosis* 70S ribosome was visualized using single-particle cryo–electron microscopy (cryo-EM) (Fig. 5 and fig. S4). Our cryo-EM reconstruction at 2.33 Å resolution clearly showed a cryo-EM density, corresponding to the **KU13** molecule, situated in the narrower region of the NPET, a location that is in close proximity to the nascent amino acid moiety on the CCA-end of the tRNA accommodated in the P site (Fig. 5B). The extended glucose-tercyclic motif of **KU13** induced a structural rearrangement in the NPET. In the previously reported structure of the *M. tuberculosis* 70*S* ribosome without a nascent peptide, U2847 (U2609 by *E. coli* numbering), a residue that is not known to form an interaction with the nascent polypeptide, makes a hydrogen bond with A881 (*46*) (A752 by *E. coli* numbering) (Fig. 5C and fig. S5). In *E. coli*, these two residues form a base pair and modulate the ribosomal response to the nascent peptide. This base pair also is involved in the bactericidal effects of extended macrolides such as TEL (*43*, *47*). This base pair conformation is highly conserved in diverse microorganisms, including *Mycobacterium* and other clinically important bacterial pathogens (*46*, *48*–*51*) (fig. S5). However, in our **KU13**-bound structure, U2847 exhibited a nearly 180° rotation around the axis of the RNA backbone, disrupting the hydrogen bond otherwise seen between the residues forming this base pair. This rotation provided an additional π-π stacking interaction with the pyridine ring of the tercyclic motif of **KU13** (Fig. 5D). On the other side of U2847, G2846 (G2608 by *E. coli* numbering) was seen to form another interaction with **KU13**. That is, the pyridine ring of **KU13** was effectively sandwiched between U2847 and G2846 (Fig. 5D) in the cryo-EM structure. The benzene ring of the tercyclic moiety appeared to form π-π interaction with U2016 (U1782 by *E. coli* numbering) as well, further enhancing the binding of the C-11 substituent to the ribosome (Fig. 5D). These interactions are inferred to play an important role in ribosomal binding by **KU13**, providing a robust anchor for the antibiotic association with the ribosome. This structural enhancement of macrolide binding to the NPET explains the higher activity of this derivative in translation inhibition in the cell-free translation system (Fig. 4). The structural comparison with previously reported macrolide-bound ribosomes (*52*) revealed that the AZM

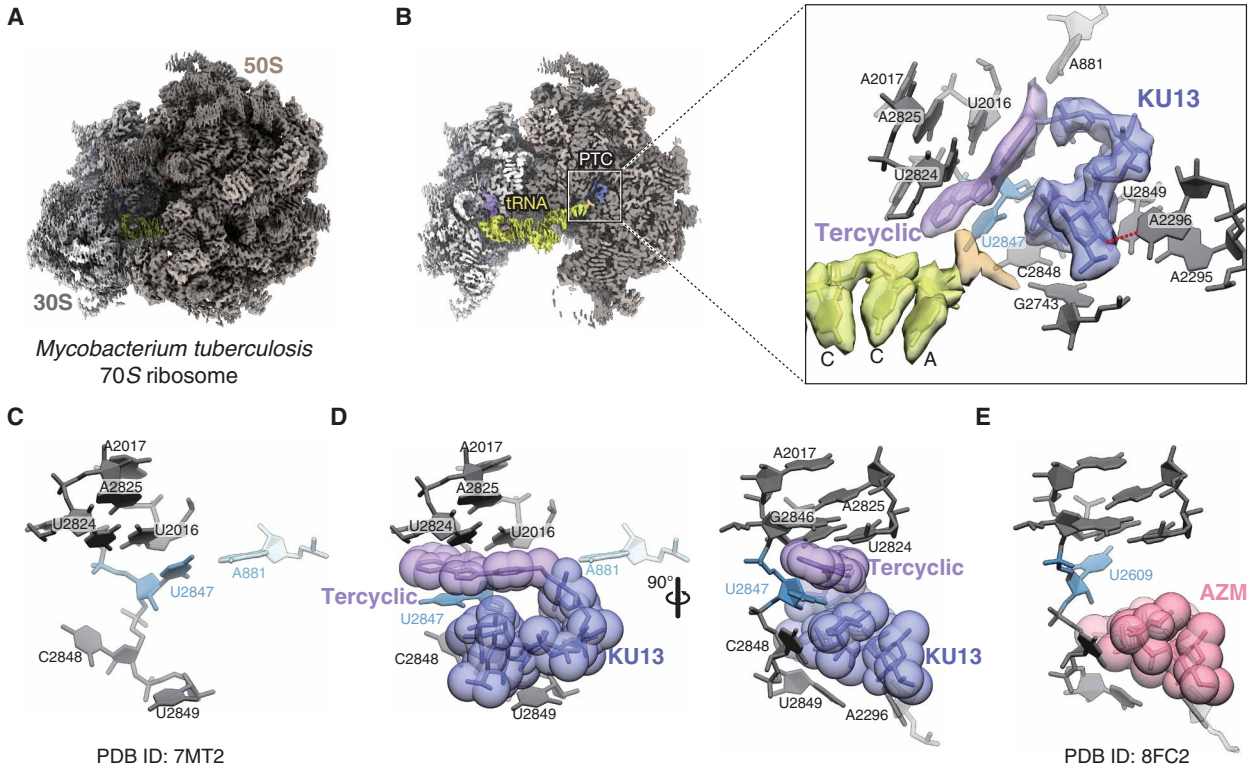

Fig. 5. Cryo-EM structure of the KU13-bound *M. tuberculosis* 70S ribosome. (**A**) Cryo-EM reconstruction of the **KU13**-bound *M. tuberculosis* 70*S* ribosome. (**B**) A cross section of (A) showing the internal regions of the ribosome. The cryo-EM density corresponding to **KU13** is observed in the area of the NPET close to the peptidyl transferase center (PTC). The enlarged view on the right panel shows the **KU13** density, with the compound's ribosomal environment shown: **KU13** (blue), tercyclic motif of **KU13** (purple), tRNA (yellow green), nascent peptide (gold), rRNA (gray). Hydrogen bonds are indicated as a red dotted line. (**C**) The *M. tuberculosis* 70*S* **KU13** binding pocket in the absence of **KU13** (PDB ID: 7MT2) (*46*). Note that U2847 is situated proximal to U2016. (**D**) The *M. tuberculosis* 70*S* **KU13** binding pocket in the presence of **KU13** (as determined in the present study). Note that U2847 here is rotated by approximately 180° relative to the unbound state shown in (C). (**E**) AZM-bound *Thermus thermophilus* 70*S* ribosome (PDB ID: 8FC2) (*52*). Note that U2609 (corresponding to *M. tuberculosis* U2847) is not rotated upon the binding of AZM without tercyclic modification. The rRNA sequence forming the binding pocket between these species is conserved.

portion of **KU13** forms interactions with ribosomal environments in a manner similar to that seen with AZM itself (Fig. 5, D and E, and fig. S6). In this context, we note that the ribosomal environments are fully conserved across the *Mycobacterium* complex and in other bacteria, except that the AU interaction of the A2295-U2849 base pair is replaced with a GC interaction (fig. S5). The adenosine at position 2296 (A2058 by *E. coli* numbering) is known to be essential for macrolide binding to the bacterial ribosome. In our **KU13**-bound structure, A2296 forms a hydrogen bond with the desosamine moiety of **KU13**, in parallel to the binding seen with AZM itself (Fig. 5, D and E).

Considered together, our results showed that **KU13** binds to the ribosome environment in the NPET via a synthetic tailored glucose-tercyclic motif, forming a robust anchor with an induced fit provided by the flipping of U2847. In addition, the conserved AZM motif also makes a strong interaction, including hydrogen bond formation with A2296, which is essential for macrolide binding.

DISCUSSION

The development of antibiotics is highly urgent, given that the emergence of antimicrobial resistance (AMR) has begun to render our current arsenal of antibiotics less effective (*53*, *54*). In general, resistance to antibiotics that target the ribosome depends on the chemical inactivation of the compounds or modifications that alter antibiotic-binding pockets on ribosomes. These changes ultimately attenuate the binding of such antibiotics to targets on the bacterial ribosome (*55*). Therefore, one approach to developing antibiotics that overcome drug resistance is to synthetically design the anchors used by these compounds (*56*). In this context, the functional and structural evaluation of semi-synthetically generated antibiotics is essential.

To design a large variety of ribosome-targeting anchors based on a common strategy, we applied our late-stage BMAD method for the chemical modification of AZM. Specifically, we used BMAD to introduce chemical modifications at a desired site in AZM, permitting us to generate AZM derivatives with selective antimicrobial activity against the recently emerging MAC (Fig. 3). First, we developed the late-stage BMAD method to selectively introduce various sugar moieties at the C-11 of AZM. The BMAD reaction facilitated modification exclusively at C-11, permitting synthesis of the AZM derivatives **KU01** to **KU05** with excellent regio- and stereoselectivity. Second, we applied this method in an efficient three-step sequence of (i) late-stage BMAD reaction, (ii) deprotection reaction, and (iii) Huisgen cycloaddition, providing the synthesis of AZM derivatives with azido or triazole substituents at C-11. As a result, **KU06** to **KU13** were successfully synthesized, completing the library of AZM derivatives **KU01** to **KU13**.

Next, **KU01** to **KU13** were evaluated for whole-cell antimicrobial activity against species of *Mycobacteria* and multiple strains of *E. coli* (Table 1). The results demonstrated that **KU13** exhibits potent antimicrobial activity against both wild-type and macrolide-resistant MAC, as well as against *M. tuberculosis*. To elucidate the mechanism underlying the enhanced activity of **KU13**, we initially investigated the impact on translation inhibition of inserting the glucose-tercyclic moiety in AZM, specifically by evaluating GFP protein production in the cell-free PURE system (Fig. 4). A comparison of the translation inhibition activities of AZM and **KU13** revealed the demonstrably superior activity of **KU13**, confirming that **KU13**'s activity targets the ribosome. Subsequently, we used cryo-EM to obtain structural insights into the mechanism by which **KU13** achieves its superior translation inhibition activity. In our cryo-EM reconstruction, the tercyclic motif of **KU13** successfully formed an anchor with 23*S* rRNA (Fig. 5). **KU13** binding disrupted a hydrogen bond formed between A881 and U2847 of the 23*S* rRNA while flipping U2847 to create a unique binding pocket in which U2847 (in combination with G2846) accommodates the tercyclic motif, forming a π-π stacking interaction between the pyridine ring of **KU13** and U2847, as well as between the same pyridine ring and G2846, and between benzene ring of **KU13** and U2016. This "induced-fit" binding mode differs from that seen for previously reported ketolides, such as TEL and solithromycin (*57*, *58*). The stable base pairing between A881 and U2847 (A752 and U2609 by *E. coli* numbering) is essential for the binding of the alkyl-aryl side chain of TEL and solithromycin (fig. S7) (*43*, *47*). Thus, this chemical insertion of a ketolide is situated in the opposite direction of that used by **KU13** (fig. S7B). The binding of TEL and solithromycin do not cause structural rearrangements, and analogous antibiotics bind to the naturally formed preexisting binding pocket on the ribosome. Our approach using the BMAD method permitted the successful design of an anchor, such that one of our derivatives generates a target binding site by inducing a structural rearrangement within the ribosome, causing U2847 to flip by approximately 180° (Fig. 5). The formation of a hydrogen bond between A2296 (A2058 by *E. coli* numbering) and the desosamine sugar of the macrolide backbone is essential for the binding of this antibiotic class to the bacterial ribosome. Macrolide-resistant bacterial pathogens often harbor modifications at this key site, including modification by methylation or point mutation to guanine (*55*). On the other hand, **KU13** has an alternative anchor for binding to the ribosome, suggesting that macrolides incorporating this moiety will exhibit potentiation of ribosomal binding. This enhancement presumably is the source of the increased translation inhibition activity observed for **KU13** (compared to AZM). Furthermore, this anchor also may explain the superior antibacterial activity of **KU13** as demonstrated in the MIC assay (Table 1), in which **KU13** exhibited a two-fold decrease in MIC (compared to AZM) against wild type *M. intracellulare*. Moreover, the anchor between the tercyclic motif and rRNA compensated for the loss of the interaction between desosamine and rRNA residue A2296 (A2058 by *E. coli* numbering) in the resistant strain. The replacement of A2058 with C in the resistant strain may result in the loss of a hydrogen bond interaction with the desosamine moiety. Thus, the MIC of AZM against a macrolide-resistant A2058C mutant of *M. intracellulare* (*M. intracellulare* B-1639) was increased (compared to the wild-type strain) to >32 μg ml^{-1}, while **KU13** had an MIC of 8 μg ml^{-1} against the macrolide-resistant strain, a value more than four-fold lower than that of AZM. We attribute this potentiation of antibiotic activity to the newly formed additional interaction between the ribosome and **KU13**'s tercyclic motif, thereby compensating for the loss of the hydrogen bond otherwise formed between the wild-type ribosome and the desosamine moiety of macrolides.

Another anticipated developmental approach for AMR is "pathogen-specific" treatment (*56*). The current preference for broad-spectrum antibiotics targets motifs that are shared among bacterial ribosomes, resulting in drastic changes to the general microbiome of the patient. However, given the increasing concern regarding specific classes of pathogenic bacteria such as ESKAPE (a mnemonic for a group of organisms that includes *Enterococcus faecium*, *Staphylococcus aureus*, *Klebsiella pneumoniae*, *Acinetobacter baumannii*, *Pseudomonas aeruginosa*, and *Enterobacter* spp.), the development and use

of antibiotics with a narrower spectrum is anticipated (*39*). MIC experiments against a range of bacterial pathogens revealed that **KU13** exhibits selective antibiotic activity against *Mycobacterium* complexes. This spectrum suggests that **KU13** would be useful for targeting the emerging MAC disease.

In conclusion, our BMAD method permitted the successful introduction of a tercyclic motif (via insertion of a glucose moiety) into the AZM backbone. As we demonstrated in the present work, this chemical modification acts as an additional anchor for binding to the bacterial ribosome and induces a structural rearrangement in the NPET of the ribosome to generate a unique binding pocket. Together, our findings suggest that **KU13** should be further explored as a promising lead compound for the development of therapeutics with activity against macrolide-resistant MAC.

MATERIALS AND METHODS

Evaluation of antibacterial activity against mycobacteria

The type strain of *M. avium*, ATCC 25291, was obtained from the American Type Culture Collection (ATCC; Manassas, VA, USA); the type strain of *M. intracellulare*, JCM 6384, was obtained from the RIKEN BioResource Research Center (Tsukuba, Japan); the type strain of *M. tuberculosis* var. BCG Tokyo 172-2 was provided from National Institute of Infectious Diseases (Japan). Strains B-1657 and B-1639 were selected as single colonies with macrolide resistance from cultures of ATCC 25291 and JCM 6384, respectively, following growth on Middlebrook 7H10 agar supplemented with OADC enrichment containing erythromycin. The sequences of the 23*S* rRNA genes in these macrolide-resistant strains were verified by Sanger sequencing, revealing mutations from adenine to cytosine at positions 2059 and 2058 (*E. coli* numbering), respectively.

The MIC values of AZM and its derivatives were determined by a serial microbroth dilution method. The mycobacterial cells were diluted to a density of approximately 10^6 colony-forming units (CFU) ml^{-1} in Middlebrook 7H9 broth that had been adjusted to a pH of 7.4 and supplemented with ADC enrichment. The cell suspensions then were exposed to serial dilutions of compounds and incubated at 37°C for 14 days. The lowest concentration at which cell growth was completely absent (as judged by visual inspection) was defined as the MIC. Middlebrook 7H10 agar, Middlebrook 7H9 broth, OADC enrichment, and ADC enrichment were obtained from Becton, Dickinson and Company (Franklin Lakes, NJ, USA).

Evaluation of antibacterial activity against other gram-positive and gram-negative bacteria

Test strains shown in Table 1 (other than *Mycobacterium*) and table S2 are laboratory collection in Institute of Microbial Chemistry, except for those listed below; *S. aureus* Mu50 was provided from K. Hiramatsu, formerly of Juntendo University. *E. coli* CAG12184 was obtained from National BioResource Project: *E. coli*, National Institute of Genetics (Shizuoka, Japan). *Neisseria gonorrhoeae* DSM9188 was purchased from the German Collection of Microorganisms and Cell Cultures (DSMZ; Lower Saxony, Germany). *N. gonorrhoeae* Z3176 is a derivative strain of DSM 9188, in which the C2611 to U mutations (using *E. coli* numbering) have been genetically introduced in all four 23*S* rRNA genes. *N. gonorrhoeae* Z2475 is same as Z3176 but the mutations are A2059 to G.

The MIC values were examined by a serial agar dilution method according to Clinical and Laboratory Standards Institute guidelines (*59*). The test-organism suspension was prepared at approximately 10^4 CFU per spot using a MIC-2000 (Dynatech Laboratories, Inc.) inoculum replicating apparatus. The MIC was defined as the lowest concentration of antibiotic that inhibited development of visible growth on the agar after 18 hours of incubation at 37°C (42 hours of incubation at 37°C for *M. smegmatis*). Compounds were dissolved in DMSO. Appropriate dilutions were made with the required culture medium immediately before testing.

Ribosome purification

E. coli ribosomes were purified from Strain KT101 (*60*). In brief, a culture (100 ml) of KT101, grown to an absorbance at 600 nm of 0.5, was harvested by centrifugation. The resulting bacterial pellet was suspended in 1 ml of lysis buffer [20 mM HEPES-KOH (pH 7.6), 10 mM $Mg(OAc)_2$, and 30 mM NH_4Cl]. The cells were disrupted by the addition of lysozyme (10 μl of a 50-mg/ml solution) to the cell suspension, which was mixed well, frozen in liquid nitrogen, and gently thawed. The resulting lysate was centrifuged at 20,000*g* for 10 min to remove debris. The cleared lysate then was subjected to sucrose density gradient centrifugation using an SW28 centrifuge rotor (Beckman Coulter, Brea, CA, USA) at 28,000 rpm for 4.5 hours in a 10 to 40% (w/v) sucrose gradient formulated in the above lysis buffer. The 70*S* ribosome fraction was isolated using a Gradient Master (BioComp, San Antonio, TX, USA).

M. tuberculosis ribosomes were purified from the *M. tuberculosis* var. BCG Pasteur strain, purchased from ATCC. This strain lacks the macrolide-resistant gene *erm* (*37*), which encodes an rRNA methyltransferase and is found in other *M. tuberculosis* strains (*61*). In brief, a culture (7.6 liters) of BCG Pasteur, grown to an absorbance at 540 nm of 0.1, was harvested by centrifugation. Cells in the resulting bacterial pellet were disrupted mechanically using a motor and aluminum oxide powder. The disrupted cells were centrifuged to remove the aluminum oxide and cell debris. *M. tuberculosis* 70*S* ribosomes then were purified using sucrose density gradient centrifugation as described above for *E. coli* ribosomes.

In vitro translation inhibition assay

The in vitro translation inhibition assay was performed using the PURExfrex reconstituted in vitro translation system 1.0 (GeneFrontier Corp., Chiba, Japan) according to the manufacturer's instructions, except that Solution III was replaced with ribosomes purified (as described above) from *E. coli* KT101. The mRNA for the *sfGFP* reporter gene (encoding Superfolder GFP) was synthesized using the in vitro Transcription T7 Kit (for siRNA Synthesis) (Takara Bio, Shiga, Japan) (*42*). In brief, for the assay itself, PURExfrex Solutions I and II were combined with ribosomes and 0 to 1000 nM of **KU13** or AZM. The *sfGFP* mRNA (30 ng/μl) then were added to the mixture, and the reaction was incubated at 37°C for 120 min, with sampling at intermediate time points. The levels of sfGFP synthesized were monitored by measuring fluorescence (excitation/emission wavelengths, 485/510 nm, respectively) using a Varioskan LUX instrument (Thermo Fisher Scientific Inc., Waltham, MA). In vitro translation inhibition assays were performed in triplicate, and the averaged values were plotted with their SD.

Cryo-EM grid preparation and data collection

To form the antibiotic-bond ribosome complex, 10 μM **KU13** was added to 100 nM *M. tuberculosis* 70*S*. A 3-μl portion of the **KU13**-bound *M. tuberculosis* 70*S* complex at 100 nM was applied to a

glow-discharged Quantifoil R1.2/1.3 200-mesh Cu grid (Quantifoil, Jena, Germany) that had previously been coated with a continuous amorphous carbon film using a JEE-420 vacuum evaporator (JEOL, Tokyo, Japan). Immediately following sample application, grids were blotted with filter paper to remove the excess solution and flash-frozen by plunging into liquid ethane using a Vitrobot Mark IV (Thermo Fisher Scientific). Cryo-EM images were obtained with a CRYO ARM 300 II electron microscope (JEOL) operating at an accelerating voltage of 300 kV; images were recorded with a K3 camera (Gatan Inc., Pleasanton, CA, USA) at a nominal magnification of 60,000×, corresponding to an objective pixel size of 0.788 Å. The defocus range of the data collection extended from −0.3 to −3.0 μm. The total exposure dose on the specimen was 40 $e^{-}/Å^{-2}$, and each exposure was fractioned into 40 and recorded as movie frames. Automated data acquisition was performed using the Serial EM program (*62*).

Single-particle image processing and model building

Single-particle image processing was performed using the RELION 4.0 program (*63*). A total of 3724 movie micrographs were motion corrected and dose weighted using the program implemented in RELION 4.0 (fig. S4). These motion-corrected micrographs showed distinct ribosome particles (fig. S4B). Contrast transfer function (CTF) parameters of the motion-corrected micrographs were estimated using the CTFFIND 4.1 program (*64*). Ribosome-particle images were picked using the AutoPick function implemented in RELION 4.0. A total of 515,051 extracted particles were classified using two-dimensional (2D) classification to discard junk particles. The resulting selection of 366,623 particles was autorefined to obtain a consensus reconstruction. Subsequently, 3D classification was performed on the basis of the alignment information of the consensus reconstruction. The major class, containing 205,461 particles, underwent autorefinement, CTF refinement, Bayesian polishing, and a further round of autorefinement, yielding a cryo-EM reconstruction at a resolution of 2.33 Å (fig. S4C). The local resolution distribution of the cryo-EM structure was calculated with the program implemented in RELION 4.0 (fig. S4D). The structural model was constructed using UCSF Chimera (*65*) and COOT (*66*) with a starting model composed of the structure of *M. tuberculosis* 70*S* [Protein Data Bank (PDB) ID: 7MT2] (*46*). The composed model, including **KU13**, was real-space refined using phenix.real_space_refine routine in the PHENIX package (*67*). The structural validation of the final model was assessed using MOLPROBITY (*68*) (table S3). Graphical figures were prepared using UCSF Chimera (*65*) and UCSF Chimera X (*69*).

Supplementary Materials

This PDF file includes:

Figs. S1 to S83
Tables S1 to S3
Supplementary Methods
References

REFERENCES AND NOTES

1. K. To, R. Cao, A. Yegiazaryan, J. Owens, V. Venketaraman, General overview of nontuberculous mycobacteria opportunistic pathogens: *Mycobacterium avium* and *Mycobacterium abscessus*. *J. Clin. Med.* **9**, 2541 (2020).
2. C. Piersimoni, C. Scarparo, Pulmonary infections associated with non-tuberculous mycobacteria in immunocompetent patients. *Lancet Infect. Dis.* **8**, 323–334 (2008).
3. H. Namkoong, A. Kurashima, K. Morimoto, Y. Hoshino, N. Hasegawa, M. Ato, S. Mitarai, Epidemiology of pulmonary nontuberculous mycobacterial disease, Japan. *Emerg. Infect. Dis.* **22**, 1116–1117 (2016).
4. M. Lipman, J. Cleverley, T. Fardon, B. Musaddaq, D. Peckham, R. van der Laan, P. Whitaker, J. White, Current and future management of non-tuberculous mycobacterial pulmonary disease (NTM-PD) in the UK. *BMJ Open Respir. Res.* **7**, e000591 (2020).
5. C. L. Daley, J. M. Iaccarino, C. Lange, E. Cambau, R. J. Wallace Jr., C. Andrejak, E. C. Böttger, J. Brozek, D. E. Griffith, L. Guglielmetti, G. A. Huitt, S. L. Knight, P. Leitman, T. K. Marras, K. N. Olivier, M. Santin, J. E. Stout, E. Tortoli, J. van Ingen, D. Wagner, K. L. Winthrop, Treatment of nontuberculous mycobacterial pulmonary disease: An official ATS/ERS/ESCMID/IDSA clinical practice guideline. *Clin. Infect. Dis.* **71**, e1–e36 (2020).
6. H.-J. Kim, J. S. Lee, N. Kwak, J. Cho, C.-H. Lee, S. K. Han, J.-J. Yim, Role of ethambutol and rifampicin in the treatment of *Mycobacterium avium* complex pulmonary disease. *BMC Pulm. Med.* **19**, 212–221 (2019).
7. C. Lange, E. C. Böttger, E. Cambau, D. E. Griffith, L. Guglielmetti, J. van Ingen, S. L. Knight, T. K. Marras, K. N. Olivier, M. Santin, J. E. Stout, E. Tortoli, D. Wagner, K. Winthrop, C. L. Daley, Expert Panel Group for Management Recommendations in Non-tuberculous Mycobacterial Pulmonary Diseases, Consensus management recommendations for less common non-tuberculous mycobacterial pulmonary diseases. *Lancet Infect. Dis.* **22**, e178–e190 (2022).
8. Y. Gu, W. Nie, H. Huang, X. Yu, Non-tuberculous mycobacterial disease: Progress and advances in the development of novel candidate and repurposed drugs. *Front. Cell. Infect. Microbiol.* **13**, 1243457 (2023).
9. Y. Park, E. H. Lee, I. Jung, G. Park, Y. A. Kang, Clinical characteristics and treatment outcomes of patients with macrolide-resistant *Mycobacterium avium* complex pulmonary disease: A systematic review and meta-analysis. *Respir. Res.* **20**, 286 (2019).
10. N. Vázquez-Laslop, A. S. Mankin, Context-specific action of ribosomal antibiotics. *Annu. Rev. Microbiol.* **72**, 185–207 (2018).
11. A. R. Davis, D. W. Gohara, M.-N. F. Yap, Sequence selectivity of macrolide-induced translational attenuation. *Proc. Natl. Acad. Sci. U.S.A.* **111**, 15379–15384 (2014).
12. J. A. Dunkle, L. Xiong, A. S. Mankin, J. H. D. Cate, Structures of the *Escherichia coli* ribosome with antibiotics bound near the peptidyl transferase center explain spectra of drug action. *Proc. Natl. Acad. Sci. U.S.A.* **107**, 17152–17157 (2010).
13. S. Saxena, H. P. Spaink, G. Forn-Cuní, Drug resistance in nontuberculous mycobacteria: Mechanisms and models. *Biology* **10**, 96 (2021).
14. M. J. Nasiri, M. Haeili, M. Ghazi, H. Goudarzi, A. Pormohammad, A. A. Imani Fooladi, M. M. Feizabadi, New insights in to the intrinsic and acquired drug resistance mechanisms in mycobacteria. *Front. Microbiol.* **8**, 681 (2017).
15. X.-Z. Li, L. Zhang, H. Nikaido, Efflux pump-mediated intrinsic drug resistance in *Mycobacterium smegmatis*. *Antimicrob. Agents Chemother.* **48**, 2415–2423 (2004).
16. M. Morar, K. Pengelly, K. Koteva, G. D. Wright, Mechanism and diversity of the erythromycin esterase family of enzymes. *Biochemistry* **51**, 1740–1751 (2012).
17. M. Arthur, P. Courvalin, Contribution of two different mechanisms to erythromycin resistance in *Escherichia coli*. *Antimicrob. Agents Chemother.* **30**, 694–700 (1986).
18. J. van Ingen, M. J. Boeree, D. van Soolingen, J. W. Mouton, Resistance mechanisms and drug susceptibility testing of nontuberculous mycobacteria. *Drug Resist. Updat.* **15**, 149–161 (2012).
19. B. Vester, S. Douthwaite, Macrolide resistance conferred by base substitutions in 23S rRNA. *Antimicrob. Agents Chemother.* **45**, 1–12 (2001).
20. A. Denis, C. Agouridas, J. M. Auger, Y. Benedetti, A. Bonnefoy, F. Bretin, J. F. Chantot, A. Dussarat, C. Fromentin, S. G. D'Ambrières, S. Lachaud, P. Laurin, O. Le Martret, V. Loyau, N. Tessot, J. M. Pejac, S. Perron, Synthesis and antibacterial activity of HMR 3647 a new ketolide highly potent against erythromycin-resistant and susceptible pathogens. *Bioorg. Med. Chem. Lett.* **9**, 3075–3080 (1999).
21. I. B. Seiple, Z. Zhang, P. Jakubec, A. Langlois-Mercier, P. M. Wright, D. T. Hog, K. Yabu, S. R. Allu, T. Fukuzaki, P. N. Carlsen, Y. Kitamura, X. Zhou, M. L. Condakes, F. T. Szczypiński, W. D. Green, A. G. Myers, A platform for the discovery of new macrolide antibiotics. *Nature* **533**, 338–345 (2016).
22. A. G. Myers, R. B. Clark, Discovery of macrolide antibiotics effective against multi-drug resistant gram-negative pathogens. *Acc. Chem. Res.* **54**, 1635–1645 (2021).
23. K. Oshima, Y. Aoyama, Regiospecific glycosylation of unprotected sugars via arylboronic activation. *J. Am. Chem. Soc.* **121**, 2315–2316 (1999).
24. C. Gouliaras, D. Lee, L. Chan, M. S. Taylor, Regioselective activation of glycosyl acceptors by a diarylborinic acid-derived catalyst. *J. Am. Chem. Soc.* **133**, 13926–13929 (2011).
25. A. Nakagawa, M. Tanaka, S. Hanamura, D. Takahashi, K. Toshima, Regioselective and 1,2-*cis*-α-stereoselective glycosylation utilizing glycosyl-acceptor-derived boronic ester catalyst. *Angew. Chemie Int. Ed. Engl.* **54**, 10935–10939 (2015).
26. M. Tanaka, J. Nashida, D. Takahashi, K. Toshima, Glycosyl-acceptor-derived borinic ester-promoted direct and β-stereoselective mannosylation with a 1,2-anhydromannose donor. *Org. Lett.* **18**, 2288–2291 (2016).
27. M. Tanaka, D. Takahashi, K. Toshima, 1,2-*cis*-α-Stereoselective glycosylation utilizing a glycosyl-acceptor-derived borinic ester and its application to the total synthesis of natural glycosphingolipids. *Org. Lett.* **18**, 5030–5033 (2016).
28. N. Nishi, J. Nashida, E. Kaji, D. Takahashi, K. Toshima, Regio- and stereoselective β-mannosylation using a boronic acid catalyst and its application in the synthesis of a

tetrasaccharide repeating unit of lipopolysaccharide derived from *E. coli* O75. *Chem. Commun.* **53**, 3018–3021 (2017).
29. M. Tanaka, A. Nakagawa, N. Nishi, K. Iijima, R. Sawa, D. Takahashi, K. Toshima, Boronic-acid-catalyzed regioselective and 1,2-*cis*-stereoselective glycosylation of unprotected sugar acceptors via S_Ni-type mechanism. *J. Am. Chem. Soc.* **140**, 3644–3651 (2018).
30. J. Nashida, N. Nishi, Y. Takahashi, C. Hayashi, M. Igarashi, D. Takahashi, K. Toshima, Systematic and stereoselective total synthesis of mannosylerythritol lipids and evaluation of their antibacterial activity. *J. Org. Chem.* **83**, 7281–7289 (2018).
31. N. Nishi, K. Sueoka, K. Iijima, R. Sawa, D. Takahashi, K. Toshima, Stereospecific β-L-rhamnopyranosylation through an S_Ni-type mechanism by using organoboron reagents. *Angew. Chemie Int. Ed. Engl.* **57**, 13858–13862 (2018).
32. M. Tanaka, K. Sato, R. Yoshida, N. Nishi, R. Oyamada, K. Inaba, D. Takahashi, K. Toshima, Diastereoselective desymmetric 1,2-*cis*-glycosylation of meso-diols via chirality transfer from a glycosyl donor. *Nat. Commun.* **11**, 2431 (2020).
33. K. Inaba, M. Endo, N. Iibuchi, D. Takahashi, K. Toshima, Total synthesis of terpioside B. *Chem. A Eur. J.* **26**, 10222–10225 (2020).
34. S. Tomita, M. Tanaka, M. Inoue, K. Inaba, D. Takahashi, K. Toshima, Diboron-catalyzed regio- and 1,2-*cis*-α-stereoselective glycosylation of *trans*-1,2-diols. *J. Org. Chem.* **85**, 16254–16262 (2020).
35. K. Inaba, Y. Naito, M. Tachibana, K. Toshima, D. Takahashi, regioselective and stereospecific β-arabinofuranosylation by boron-mediated aglycon delivery. *Angew. Chemie Int. Ed. Engl.* **62**, e2023070 (2023).
36. K. Kimura, T. Yasunaga, T. Makikawa, D. Takahashi, K. Toshima, Efficient strategy for the preparation of chemical probes of biologically active glycosides using a boron-mediated aglycon delivery (BMAD) method. *Bull. Chem. Soc. Jpn.* **95**, 1075–1082 (2022).
37. J.-H. Tay, A. J. Argüelles, M. D. DeMars, P. M. Zimmerman, D. H. Sherman, P. Nagorny, Regiodivergent glycosylations of 6-deoxy-erythronolide B and oleandomycin-derived macrolactones enabled by chiral acid catalysis. *J. Am. Chem. Soc.* **139**, 8570–8578 (2017).
38. K. Bock, C. Pedersen, A study of ^{13}CH coupling constants in hexopyranoses. *J. Chem. Soc. Perkin Trans.* **2**, 293–297 (1974).
39. M. A. Riojas, K. J. McGough, C. J. Rider-Riojas, N. Rastogi, M. H. Hazbón, Phylogenomic analysis of the species of the *Mycobacterium tuberculosis* complex demonstrates that *Mycobacterium africanum*, *Mycobacterium bovis*, *Mycobacterium caprae*, *Mycobacterium microti* and *Mycobacterium pinnipedii* are later heterotypic synonyms of *Mycobacterium tuberculosis*. *Int. J. Syst. Evol. Microbiol.* **68**, 324–332 (2018).
40. M. A. Fischbach, C. T. Walsh, Antibiotics for emerging pathogens. *Science* **325**, 1089–1093 (2009).
41. Y. S. Polikanov, N. A. Aleksashin, B. Beckert, D. N. Wilson, The mechanisms of action of ribosome-targeting peptide antibiotics. *Front. Mol. Biosci.* **5**, 1–21 (2018).
42. J. Tomono, K. Asano, T. Chiashi, M. Suzuki, M. Igarashi, Y. Takahashi, Y. Tanaka, T. Yokoyama, Direct visualization of ribosomes in the cell-free system revealed the functional evolution of aminoglycoside. *J. Biochem.* **175**, 587–598 (2024).
43. B. Llano-Sotelo, J. Dunkle, D. Klepacki, W. Zhang, P. Fernandes, J. H. Cate, A. S. Mankin, Binding and action of CEM-101, a new fluoroketolide antibiotic that inhibits protein synthesis. *Antimicrob. Agents Chemother.* **54**, 4961–4970 (2010).
44. Y. Shimizu, A. Inoue, Y. Tomari, T. Suzuki, T. Yokogawa, K. Nishikawa, T. Ueda, Cell-free translation reconstituted with purified components. *Nat. Biotechnol.* **19**, 751–755 (2001).
45. K. Kannan, N. Vázquez-Laslop, A. S. Mankin, Selective protein synthesis by ribosomes with a drug-obstructed exit tunnel. *Cell* **151**, 508–520 (2012).
46. Z. Cui, X. Li, J. Shin, H. Gamper, Y.-M. Hou, J. C. Sacchettini, J. Zhang, Interplay between an ATP-binding cassette F protein and the ribosome from *Mycobacterium tuberculosis*. *Nat. Commun.* **13**, 432 (2022).
47. M. S. Svetlov, S. Cohen, N. Alsuhebany, N. Vázquez-Laslop, A. S. Mankin, A long-distance rRNA base pair impacts the ability of macrolide antibiotics to kill bacteria. *Proc. Natl. Acad. Sci. U.S.A.* **117**, 1971–1975 (2020).
48. J. Hentschel, C. Burnside, I. Mignot, M. Leibundgut, D. Boehringer, N. Ban, The complete structure of the *Mycobacterium smegmatis* 70S ribosome. *Cell Rep.* **20**, 149–160 (2017).
49. E. L. Murphy, K. V. Singh, B. Avila, T. Kleffmann, S. T. Gregory, B. E. Murray, K. L. Krause, R. Khayat, G. Jogl, Cryo-electron microscopy structure of the 70S ribosome from *Enterococcus faecalis*. *Sci. Rep.* **10**, 16301 (2020).
50. Y. Halfon, A. Jimenez-Fernandez, R. La Rosa, R. Espinosa Portero, H. Krogh Johansen, D. Matzov, Z. Eyal, A. Bashan, E. Zimmerman, M. Belousoff, S. Molin, A. Yonath, Structure of *Pseudomonas aeruginosa* ribosomes from an aminoglycoside-resistant clinical isolate. *Proc. Natl. Acad. Sci. U.S.A.* **116**, 22275–22281 (2019).
51. D. Nicholson, T. A. Edwards, A. J. O'Neill, N. A. Ranson, Structure of the 70S ribosome from the human pathogen *Acinetobacter baumannii* in complex with clinically relevant antibiotics. *Structure* **28**, 1087–1100.e3 (2020).
52. C. W. Chen, N. Leimer, E. A. Syroegin, C. Dunand, Z. P. Bulman, K. Lewis, Y. S. Polikanov, M. S. Svetlov, Structural insights into the mechanism of overcoming Erm-mediated resistance by macrolides acting together with hygromycin-A. *Nat. Commun.* **14**, 4196 (2023).
53. J. O'Neill, *Antimicrobial Resistance: Tackling a Crisis for the Health and Wealth of Nations* (Wellcome Trust, London, England, 2014).
54. J. O'Neill, *Tackling Drug-Resistant Infections Globally: Final Report and Recommendations* (Wellcome Trust, London, England, 2016).
55. J. Lin, D. Zhou, T. A. Steitz, Y. S. Polikanov, M. G. Gagnon, Ribosome-targeting antibiotics: Modes of action, mechanisms of resistance, and implications for drug design. *Annu. Rev. Biochem.* **87**, 451–478 (2018).
56. T. Auerbach-Nevo, D. Baram, A. Bashan, M. Belousoff, E. Breiner, C. Davidovich, G. Cimicata, Z. Eyal, Y. Halfon, M. Krupkin, D. Matzov, M. Metz, M. Rufayda, M. Peretz, O. Pick, E. Pyetan, H. Rozenberg, M. Shalev-Benami, I. Wekselman, R. Zarivach, E. Zimmerman, N. Assis, J. Bloch, H. Israeli, R. Kalaora, L. Lim, O. Sade-Falk, T. Shapira, L. Taha-Salaime, H. Tang, A. Yonath, Ribosomal antibiotics: Contemporary challenges. *Antibiotics* **5**, 24 (2016).
57. H. Maus, G. Hinze, S. J. Hammerschmidt, T. Schirmeister, T. Basché, Conformational selection and induced fit: The behavior of two homologous proteases. *ChemistryEurope* **1**, e2023000 (2023).
58. B. Beckert, E. C. Leroy, S. Sothiselvam, L. V. Bock, M. S. Svetlov, M. Graf, S. Arenz, M. Abdelshahid, B. Seip, H. Grubmüller, A. S. Mankin, C. A. Innis, N. Vázquez-Laslop, D. N. Wilson, Structural and mechanistic basis for translation inhibition by macrolide and ketolide antibiotics. *Nat. Commun.* **12**, 4466 (2021).
59. CLSI, *Methods for Dilution Antimicrobial Susceptibility Tests for Bacteria That Grow Aerobically; Approved Standard–Eighth Edition* (Clinical and Laboratory Standards Institute, M07-A8, 2009).
60. K. Kitahara, T. Suzuki, The ordered transcription of RNA domains is not essential for ribosome biogenesis in *Escherichia coli*. *Mol. Cell* **34**, 760–766 (2009).
61. C. T. Madsen, L. Jakobsen, K. Buriánková, F. Doucet-Populaire, J. L. Pernodet, S. Douthwaite, Methyltransferase Erm(37) slips on rRNA to confer atypical resistance in *Mycobacterium tuberculosis*. *J. Biol. Chem.* **280**, 38942–38947 (2005).
62. D. N. Mastronarde, Automated electron microscope tomography using robust prediction of specimen movements. *J. Struct. Biol.* **152**, 36–51 (2005).
63. D. Kimanius, L. Dong, G. Sharov, T. Nakane, S. H. W. Scheres, New tools for automated cryo-EM single-particle analysis in RELION-4.0. *Biochem. J.* **478**, 4169–4185 (2021).
64. A. Rohou, N. Grigorieff, CTFFIND4: Fast and accurate defocus estimation from electron micrographs. *J. Struct. Biol.* **192**, 216–221 (2015).
65. E. F. Pettersen, T. D. Goddard, C. C. Huang, G. S. Couch, D. M. Greenblatt, E. C. Meng, T. E. Ferrin, UCSF Chimera—A visualization system for exploratory research and analysis. *J. Comput. Chem.* **25**, 1605–1612 (2004).
66. P. Emsley, B. Lohkamp, W. G. Scott, K. Cowtan, Features and development of Coot. *Acta Crystallogr. Sect. D Biol. Crystallogr.* **66**, 486–501 (2010).
67. P. D. Adams, P. V. Afonine, G. Bunkóczi, V. B. Chen, I. W. Davis, N. Echols, J. J. Headd, L. W. Hung, G. J. Kapral, R. W. Grosse-Kunstleve, A. J. McCoy, N. W. Moriarty, R. Oeffner, R. J. Read, D. C. Richardson, J. S. Richardson, T. C. Terwilliger, P. H. Zwart, PHENIX: A comprehensive Python-based system for macromolecular structure solution. *Acta Crystallogr. Sect. D Biol. Crystallogr.* **66**, 213–221 (2010).
68. V. B. Chen, W. B. Arendall III, J. J. Headd, D. A. Keedy, R. M. Immormino, G. J. Kapral, L. W. Murray, J. S. Richardson, D. C. Richardson, MolProbity: All-atom structure validation for macromolecular crystallography. *Acta Crystallogr. Sect. D Biol. Crystallogr.* **66**, 12–21 (2010).
69. T. D. Goddard, C. C. Huang, E. C. Meng, E. F. Pettersen, G. S. Couch, J. H. Morris, T. E. Ferrin, U. C. S. F. ChimeraX, Meeting modern challenges in visualization and analysis. *Protein Sci.* **27**, 14–25 (2018).
70. R. L. Halcomb, S. J. Danishefsky, On the direct epoxidation of glycals: Application of a reiterative strategy for the synthesis of β-linked oligosaccharides. *J. Am. Chem. Soc.* **111**, 6661–6666 (1989).
71. L. Alberch, G. Cheng, S.-K. Seo, X. Li, F. P. Boulineau, A. Wei, Stereoelectronic factors in the stereoselective epoxidation of glycals and 4-deoxypentenosides. *J. Org. Chem.* **76**, 2532–2547 (2011).
72. S. Manabe, Y. Marui, Y. Y. Ito, Total synthesis of mannosyl tryptophan and its derivatives. *Chem. A Eur. J.* **9**, 1435–1447 (2003).
73. Q. Chen, F. Kong, L. Cao, Synthesis, conformational analysis, and the glycosidic coupling reaction of substituted 2,7-dioxabicyclo[4.1.0]heptanes: 1,2-anhydro-3,4-di-O-benzyl-β-L- and β-D-rhamnopyranoses. *Carbohydr. Res.* **240**, 107–117 (1993).

Acknowledgments

Funding: This work was supported in part by Japan Society for the Promotion of Science KAKENHI Scientific Research (B) grant JP23H01966 (D.T.), Japan Science and Technology grant JPMJPR20EG (T.Y.), Japan Science and Technology Support for Pioneering Research Initiated by the Next Generation grant JPMJSP2123 (Y. Iso.), Japan Science and Technology Core Research for Evolutionary Science and Technology grant JPMJCR20R3 (D.T.), Japan Agency for Medical Research and Development Core Research for Evolutionary Science and Technology grant JP22gm1610010 (D.T.), and Shionogi Infectious Disease Research Promotion Foundation (D.T.).

The cryo–electron microscopy with the CRYO ARM 300 II (powered by Japan Agency for Medical Research and Development research grant JP20am0101095) was provided by the Advanced Research Center for Innovations in Next-Generation Medicine, Tohoku University.
Author contributions: Conceptualization: M.I., T.Y., K.T., and D.T. Methodology: Y. Iso., T.M., K.K., D.N., Y. Ish., M.I., T.Y., K.T., and D.T. Investigation: Y. Iso., T.M., K.K., D.N., M.F., C.H., Y. Ish., and T.Y. Visualization: Y. Iso., D.N., M.I., T.Y., and D.T. Supervision: Y.T., M.I., T.Y., K.T., and D.T. Writing–original draft: Y. Iso., Y. Ish., M.I., T.Y., and D.T. Writing–review and editing: Y. Iso., T.M., K.K., D.N., M.F., Y.T., C.H., Y. Ish., M.I., T.Y., K.T., and D.T. **Competing interests:** T.M., Y. Ish., M.I., K.T., and D.T. are inventors of one pending patent application related to this work (Japan Patent Application 2023-90620). The other authors declare that they have no competing interests. **Data and materials availability:** All data supporting the findings of this study are available within the paper and the Supplementary Materials or have been deposited to the indicated databases. Detailed synthetic procedures and ^{1}H- and ^{13}C-NMR spectra of compounds can be found in the Supplementary Materials. Data for biochemical experiments in this study are available at Zenodo (DOI: 10.5281/zenodo.14597769). The cryo-EM map and the corresponding atomic model have been deposited in the EMDB with identifiers EMD-61076 and PDB: 9J1M. Source data are provided with this paper.

Submitted 18 September 2024
Accepted 30 January 2025
Published 5 March 2025
10.1126/sciadv.adt2352